Geol. Mag. **141** (*2*), *2004, pp. 141–160.* © *2004 Cambridge University Press*
DOI: 10.1017/S0016756804008908 *Printed in the United Kingdom*

Evolution of the Timan–Pechora and South Barents Sea basins

N. O'LEARY, N. WHITE*, S. TULL, V. BASHILOV, V. KUPRIN, L. NATAPOV & D. MACDONALD

Bullard Laboratories, Department of Earth Sciences, Madingley Rise, Madingley Road, Cambridge CB3 0EZ, UK

(*Received* 23 July 2002; *revised version received* 3 June 2003; *accepted* 10 June 2003)

Abstract – We have analysed 129 stratigraphic sections from the Timan–Pechora basin, from its adjacent continental shelf and from the South Barents Sea basin, in order to determine whether existing models of extensional sedimentary basin formation can be applied to these intracratonic basins or whether new mechanisms of formation need to be invoked. The subsidence history of each section has been calculated using standard backstripping techniques. An inverse model, based on finite-duration lithospheric stretching, has then been used to calculate the distribution of strain rate as a function of time required to fit each subsidence profile. Results demonstrate an excellent fit between theory and observation. By combining our analysis with independent field-based and geophysical observations, we show that the Timan–Pechora basin underwent at least four phases of mild lithospheric stretching during the Phanerozoic ($\beta < 1.2$). These phases occurred in Ordovician, Late Ordovician–Silurian, Middle–Late Devonian and Permian–Early Triassic times. Growth on normal faults, episodes of volcanic activity and regional considerations provide corroborative support for the existence of all four phases. Although less well constrained, subsidence data from the South Barents Sea basin are consistent with a similar Early–Middle Palaeozoic history. The main difference is that Permian–Early Triassic extension is substantially greater than that seen onshore. This similarity implies structural connectivity throughout their respective evolutions. Finally, subsidence modelling demonstrates that rapid foreland basin formation, associated with the Uralian Orogeny, was initiated in Permo-Triassic times and is confined to the eastern margin of the Timan–Pechora basin. Coeval foreland subsidence does not occur on the eastern margin of the South Barents Sea basin, supporting the allochthonous nature of Novaya Zemlya. The most puzzling result is the existence of simultaneous lithospheric extension and foreland loading in Permian–Early Triassic times. This juxtaposition is most clearly seen within the Timan–Pechora basin itself and suggests that convective drawdown may play a role in foreland basin formation.

Keywords: sedimentary basins, extension, Timan–Pechora, strain rate, lithosphere.

1. Introduction

The nature and mechanism of intracratonic basin formation is poorly understood, and various different mechanisms have been used to explain their subsidence. In this study, we use a substantial database of well-log and other stratigraphic information to calculate the tectonic subsidence histories of two such intracratonic basins. These histories have then been used to identify the mechanisms by which these basins have formed. We are especially interested in showing how inverse theory can be used to extract quantitative information about a basin's history.

The Timan–Pechora basin is located on the north-east European–Russian platform and covers an area of 440 000 km^2, of which about 350 000 km^2 occur onshore (Fig. 1). Its western basin margin is delimited by the Timan Ridge, a NW–SE-trending Baykalian (Vendian) structure, which Zonenshain, Kuzmin & Natapov (1990) thought represented the collision of one or more small continental blocks ('Barentsia') with the East European Platform. The basin's eastern and northeastern margins are formed by the fold-and-thrust belt of the Urals which developed during the Late Carboniferous–Permian collision of the East European and Siberian blocks. The Timan–Pechora basin tapers southward to the position where the Timan Ridge and the Ural mountains converge. It broadens northwards, extending offshore into the Barents Sea where it merges with the South Barents Sea basin. The Timan–Pechora basin is divided into two broad, stable, basement highs with relatively thin (3–5 km) sedimentary cover (the so-called Izhma–Pechorskaya and Khoreyverskaya 'depressions' of Zonenshain, Kuzmin & Natapov, 1990). These highs are separated by NW–SE-trending, fault-defined, linear mobile belts which are known as the Pechoro-Kolvinskaya and Varandey-Adz'vinskaya rift zones) and which contain relatively thick (6–7 km) sedimentary successions (Fig. 2). Basement consists of metamorphosed volcanic and sedimentary rocks intruded by granites, which are exposed along the Timan Ridge and which have been drilled on selected highs in the basin interior.

* Author for correspondence: nwhite@esc.cam.ac.uk

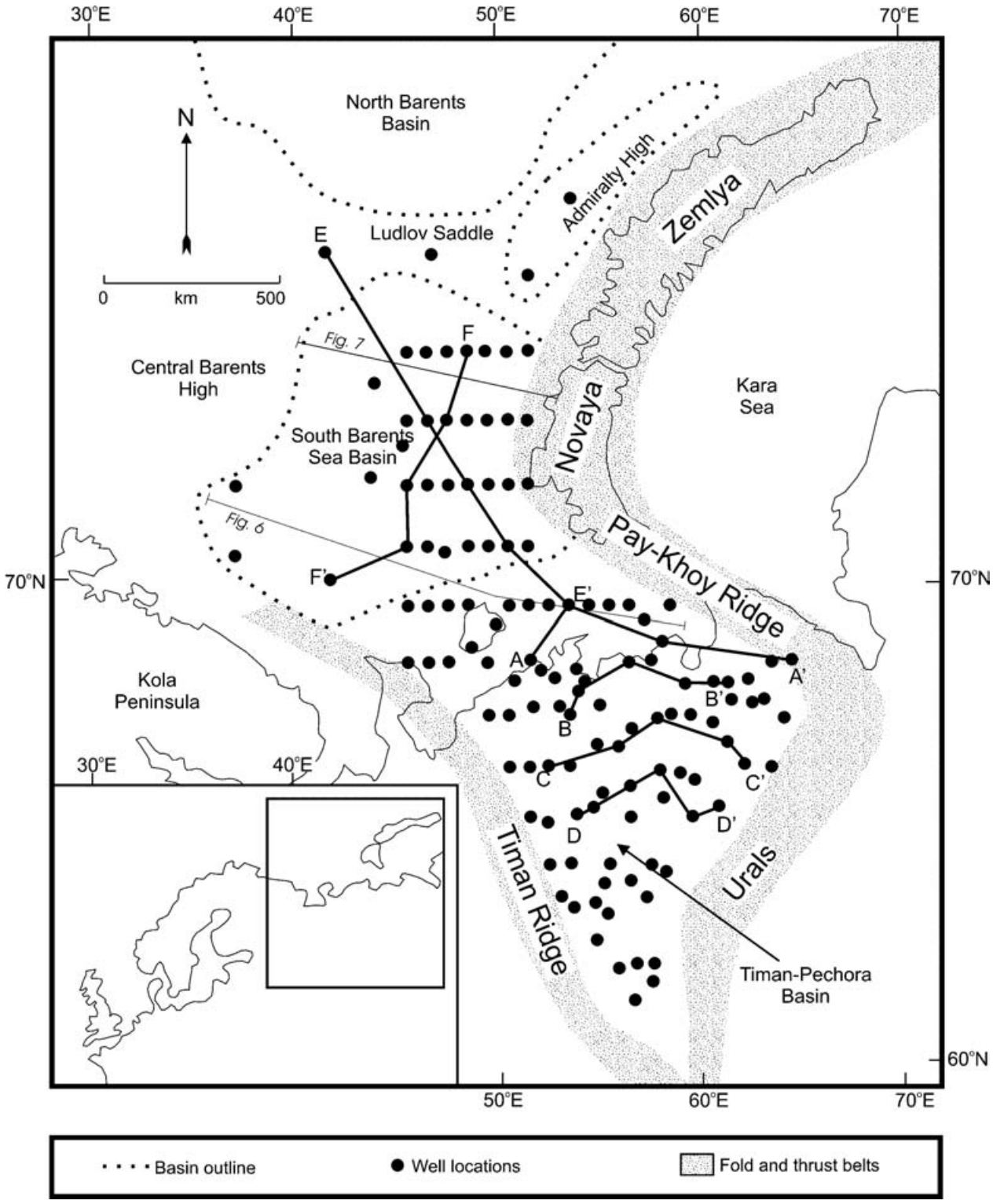

Figure 1. Map of Timan–Pechora and South Barents Sea basins showing location of dataset used in this study. Solid circles = well-log and other stratigraphic information; thick lines connecting solid circles = sets of modelled well-log and other stratigraphic data shown in Figure 9; thin lines = location of cross-sections shown in Figures 5 and 7; grey shading = location of basin-bounding fold and thrust belts.

1.a. Timan–Pechora basin

The broad-scale evolution of the Timan–Pechora basin is usually summarized by dividing the basin fill into four tectonostratigraphic sequences (Zonenshain, Kuzmin & Natapov, 1990; Fig. 3). 'Tectonostratigraphic Sequence 1' (TS1) is of Early–Middle Ordovician age and consists of up to 1500 m of paralic and shallow-marine siliciclastic rocks. Thicker sequences occur on the western slopes of the Urals, where

https://doi.org/10.1017/S0016756804008908 Published online by Cambridge University Press

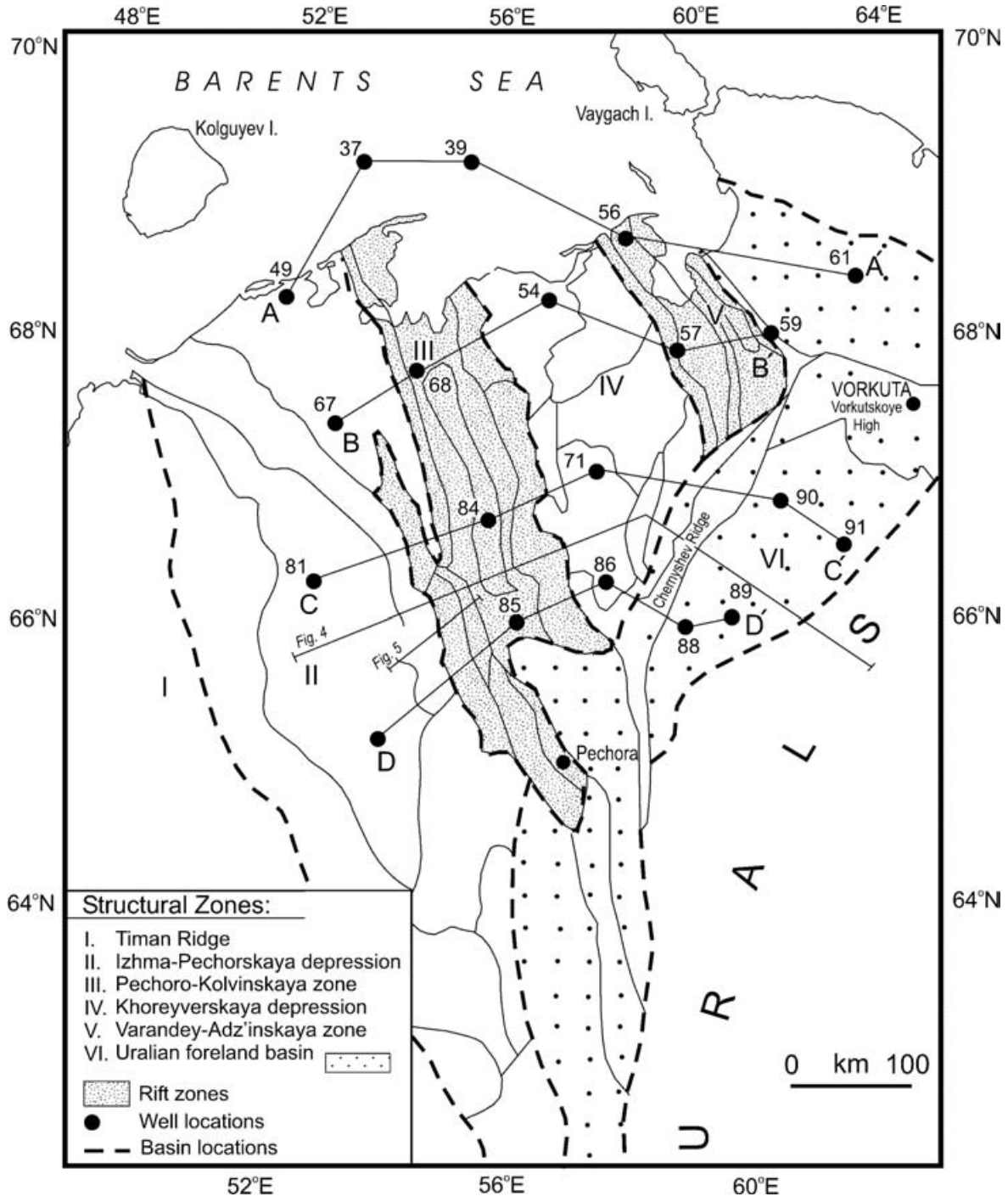

Figure 2. Map of Timan–Pechora and South Barents Sea basins showing principal structural zones (after Dedeyev, 1982). Grey shading = location of rift zones; stipple shading = Uralian foreland basin; numbered solid circles connected by labelled thin lines = transects of modelled wells and sections shown in Figure 9; dashed lines = orientation of basin swells and depressions; thin lines = location of cross-sections shown in Figures 4 and 6.

volcanic rocks are also present. A three-fold division of 'Tectonostratigraphic Sequence 2' ($TS2^1$–$TS2^3$) is based on the occurrence of Lower Devonian (Pragian–Emsian) and Lower Carboniferous (Viséan) basin-wide unconformities. The Upper Ordovician–Lower Devonian section is represented by up to 2 km of peritidal and shallow-shelf carbonates, unconformably overlain by up to 2 km of Middle Devonian continental and shallow-marine siliciclastic rocks. These sediments mainly accumulated in western and central parts of the basin (the Izhma–Pechorskaya 'depression' and the Pechoro–Kolvinskaya rift zone), and deposition was accompanied by minor basaltic volcanism. Middle Devonian sands pass up into Upper Devonian shallow-shelf carbonates and deeper marine black shales and limestones. TS2 is capped by Lower Carboniferous

https://doi.org/10.1017/S0016756804008908 Published online by Cambridge University Press

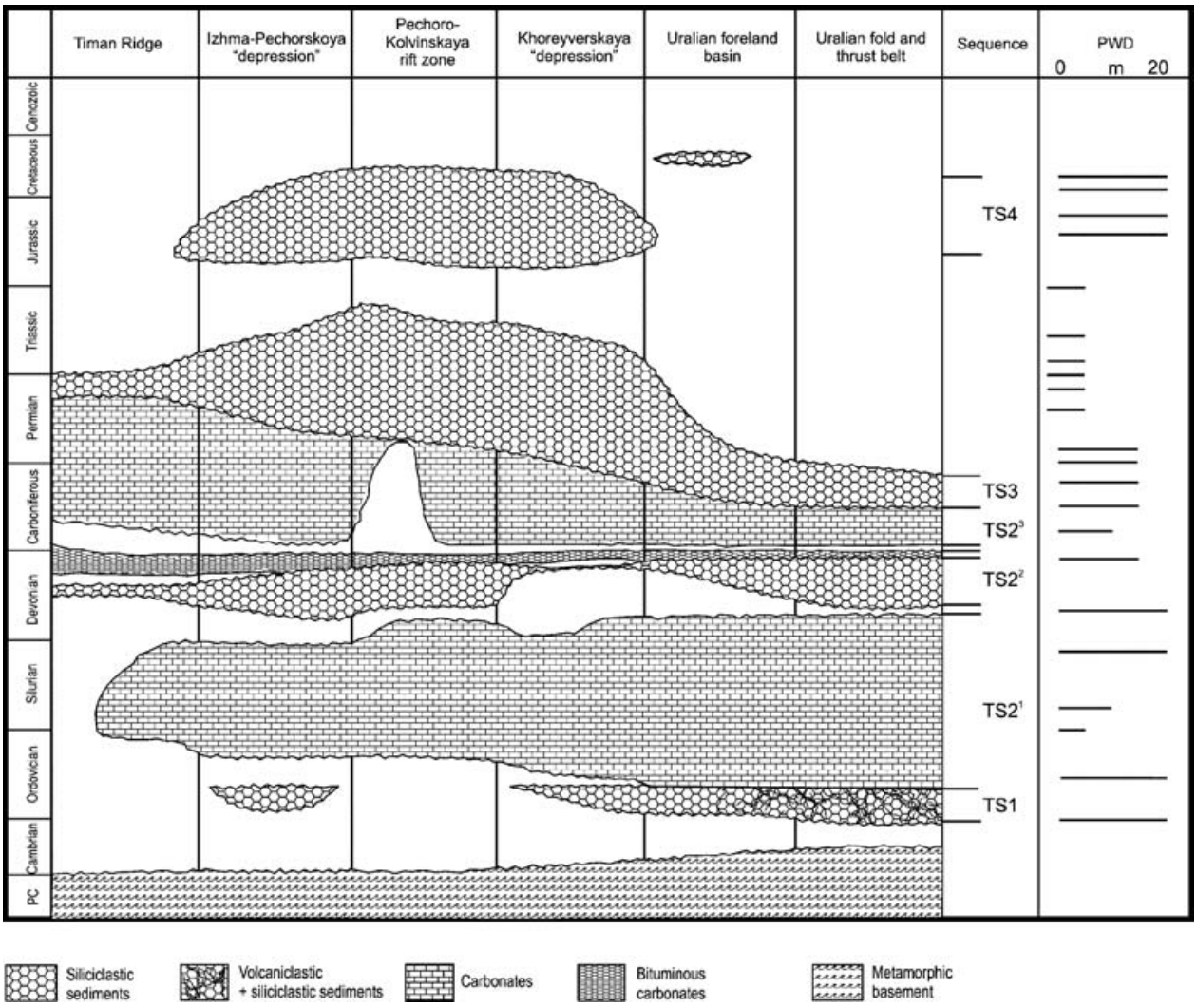

Figure 3. Simplified chronostratigraphy of Timan–Pechora basin, subdivided into structural zones illustrated in Figures 1 and 2. PWD = palaeowater depth ranges. TS1–TS4 indicate tectonostratigraphic sequences discussed in text; $TS2^1$, $TS2^2$ and $TS2^3$ refer to lower, middle and upper divisions of tectonostratigraphic sequence 2, respectively. Truncation of TS2 in Pechoro-Kolvinskaya rift zone is a consequence of uplift and denudation associated with the Uralian Orogeny.

(upper Viséan)–Lower Permian shallow-marine shelf carbonates and evaporates. The first two sequences are thought to represent the evolution of the basin on a passive continental margin. 'Tectonostratographic Sequence 3' (TS3) is of late Early Permian–Triassic age and mainly developed in response to foreland basin formation along the eastern flank of the Timan–Pechora basin during the Uralian Orogeny. Lower Permian marine siliciclastic rocks give way to Upper Permian non-marine siliciclastic rocks and coals representing the 'flysch' and 'molasse' stages of foreland basin development, respectively. This foreland basin fill is up to 5–6 km thick. Sands which overspilled the foreland basin into the platformal part of the Timan–Pechora basin were diverted northward by axial fluvial systems. Sedimentation was accompanied by basaltic volcanism during latest Permian and earliest Triassic times. 'Tectonostratigraphic Sequence 4' (TS4) consists of Jurassic–Cretaceous continental to shallow-marine siliciclastic rocks. This sequence forms much of the surface geology in the Timan–Pechora basin. Relatively thin onshore successions (maximum 800 m) thicken appreciably offshore into the South Barents basin.

The structural configuration of this pile of shallow-water sedimentary rocks is shown in Figure 4. Close to the western edge of the basin, the Ordovician–Cretaceous section is up to 4 km thick and relatively undeformed. The first major change in thickness occurs at the boundary between Zones II and III, which is marked by a series of major normal faults, across which there is stratigraphic growth. Within the central part of the basin, the stratigraphic pile reaches thicknesses of 7 km and there is evidence for growth across normal faults. The Chernyshev Ridge at the boundary between Zones IV and VI marks a

https://doi.org/10.1017/S0016756804008908 Published online by Cambridge University Press

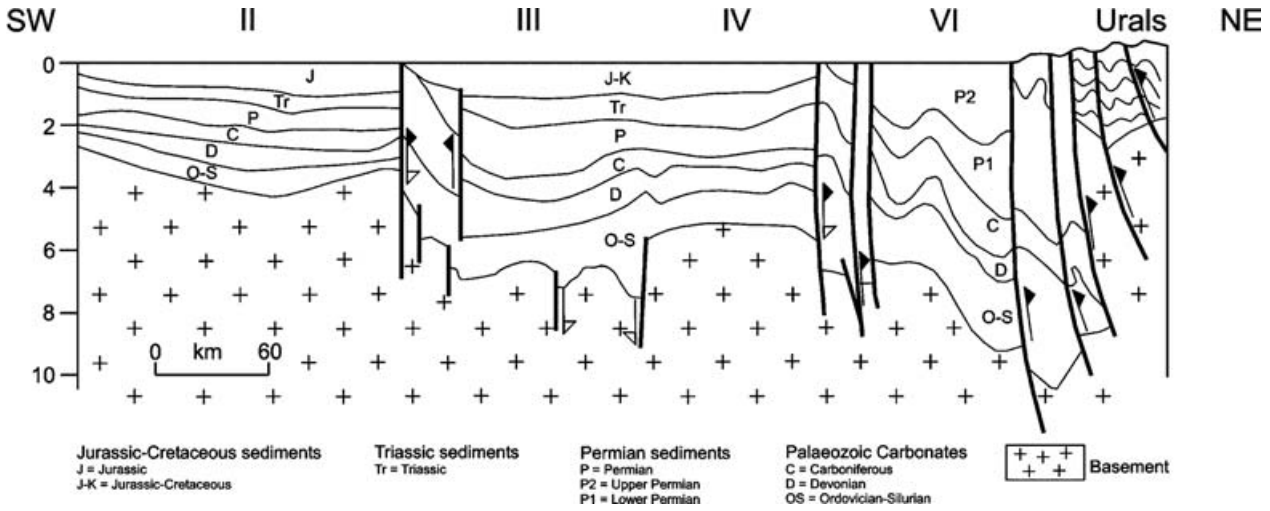

Figure 4. Generalized cross-section of Timan–Pechora basin (after Meyerhoff, 1980). Thickened Permian section at NE end represents the Uralian foreland basin. Arrows on faults give direction of slip; double arrows indicated reactivated faults (orientation of several faults is uncertain and they are shown schematically as vertical). Roman numerals = structural zones referred to in Figures 1 and 2. Vertical exaggeration × 16.

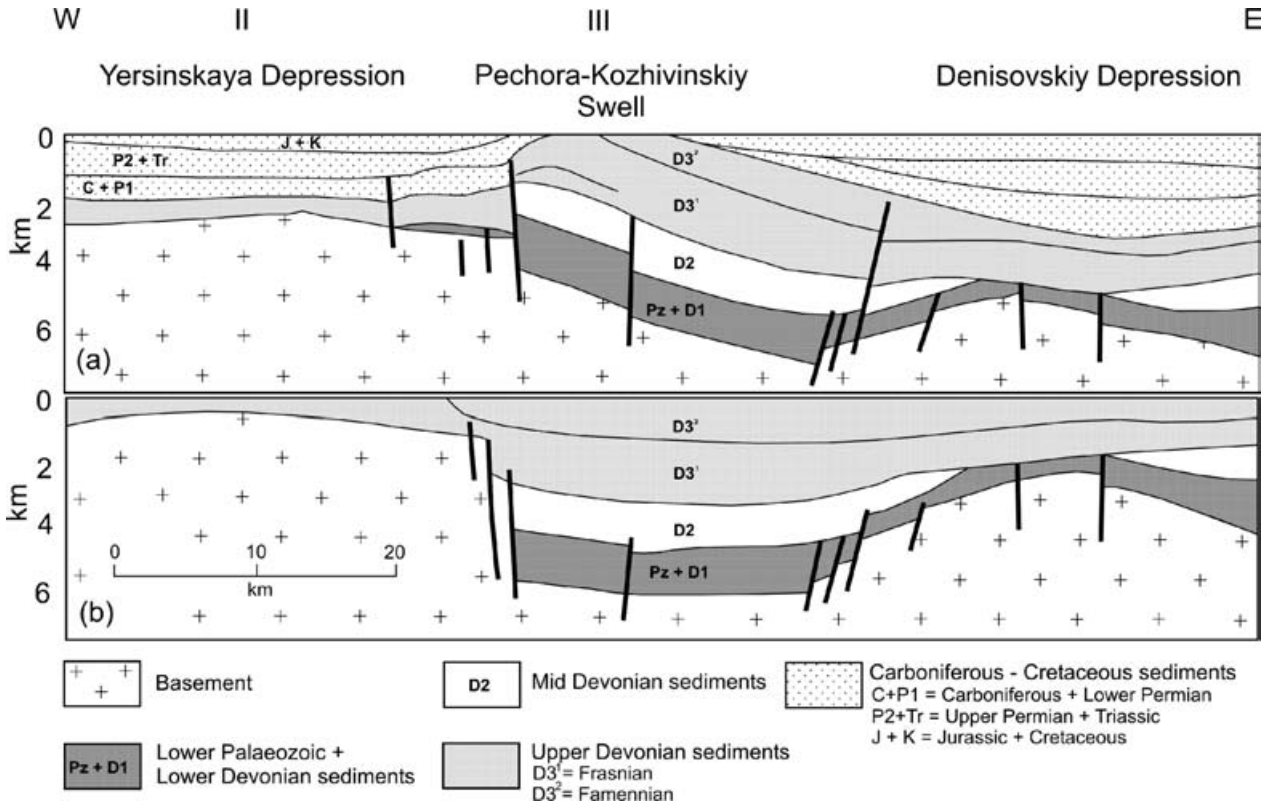

Figure 5. Cross-section showing the structure and stratigraphy of structural zones II and III at western edge of Timan–Pechora basin. Note fault-bounded growth during Early Palaeozoic/Early Devonian times and during Frasnian/Famennian times. See Figure 2 for location.

major change in deformational style. East of this ridge, the stratigraphy is deformed by thrust faulting which increases in intensity up to the Ural Mountains. The overall shape of the basin suggests that it formed by foreland loading. However, there is excellent evidence for syn-sedimentary normal faulting, especially along the western edge of the basin. The cross-sections in Figures 5, 6 and 7 show clear evidence for growth across normal faults at several stages within the Palaeozoic.

https://doi.org/10.1017/S0016756804008908 Published online by Cambridge University Press

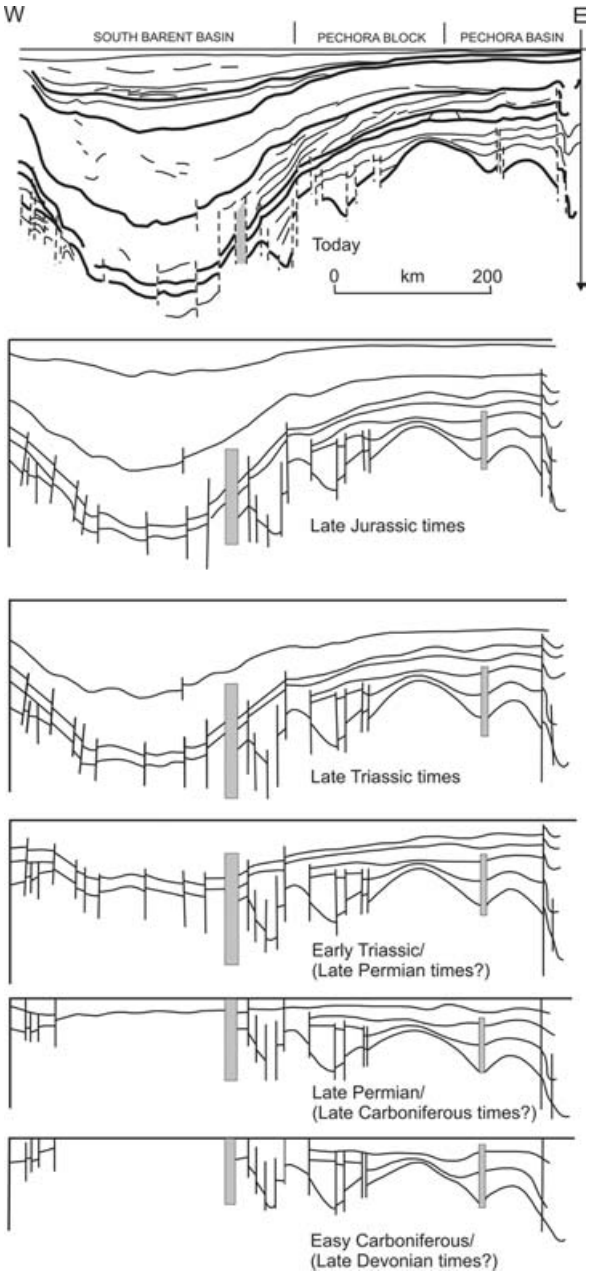

Figure 6. Cross-section showing spatial and temporal relationship between South Barents Sea and Pechora basins. The lower five panels schematically illustrate the evolution of this transect. See Figure 1 for location. Grey panels: left panel represents the eastern axis separating the South Barents Sea basin from the Pechora Block in pre-Carboniferous times; right panel indicates depocentre of Pechora basin.

1.b. South Barents Sea basin

Lack of well-log information means that the pre-Triassic geology of the South Barents Sea basin is less well known than that of the Timan–Pechora basin. An E–W fault zone forms the boundary between the two basins. This series of faults blocks contains probable Ordovician–Lower Devonian clastics and carbonates which are unconformably overlain by Upper Devonian–Lower Permian carbonate-dominated sedimentary rocks. Shallow-marine carbonates were deposited throughout the Barents region during much of Late Palaeozoic times, but in Permian times, or possibly as early as Late Carboniferous times, these are replaced by marine sandstones and mudstones in the centre of the South Barents Sea basin. The Late Permian–Early Triassic period appears to have been a time of major basin formation, with subsidence accommodating the accumulation of more than 7 km of sediments in the basin centre. The predominantly Triassic succession is overlain by paralic and shallow-marine Lower–Middle Jurassic sandstones and mudstones and by Upper Jurassic deep marine mudstones. The Cretaceous period is represented principally by Neocomian shallow-marine clastics around the basin margins and by shales in the basin interior. Upper Cretaceous–Cenozoic rocks are thin or absent, owing in part to Cenozoic uplift and denudation.

2. Subsidence database

The database consists of 129 stratigraphic sections from onshore and offshore parts of the Timan–Pechora South Barents Sea basins (Fig. 1). These sections were compiled by the Cambridge Arctic Shelf Programme (Bashilov *et al.* unpub. CASP report, 1994) and by Aerogeologiya, Moscow (N. A. O'Leary, unpub. Ph.D. thesis, Univ. Cambridge, 1996). Some stratigraphic sections are based on continuous well data (e.g. Section 13), some on interpreted thicknesses from seismic reflection profiles (e.g. Section 64) and others on a combination of the two methods (e.g. Section 52). In all cases, a complete record of subsidence from surface to basement has been reconstructed. Coverage is excellent and provides an opportunity to develop a comprehensive understanding of both basins. The database includes comprehensive information about lithological composition, sedimentary structures, biostratigraphy and depositional enviroment. We used the geological timescale of Harland *et al.* (1989) to assign chronostratigraphic ages to stratigraphic units. N. O'Leary (unpub. Ph.D. thesis, Univ. Cambridge, 1996) showed that using other timescales has a minimal effect upon our results (e.g. Berggren *et al.* 1996). The major drawback of the stratigraphic database is that Ordovician and Silurian thicknesses are poorly constrained, and this shortcoming must be borne in mind when drawing conclusions from our analyses.

3. Subsidence modelling

3.a. Data processing

The principal aim of this study is to determine to what extent the Timan–Pechora basin and the adjacent continental shelf evolved in accordance with known models of basin formation. Since there is independent

https://doi.org/10.1017/S0016756804008908 Published online by Cambridge University Press

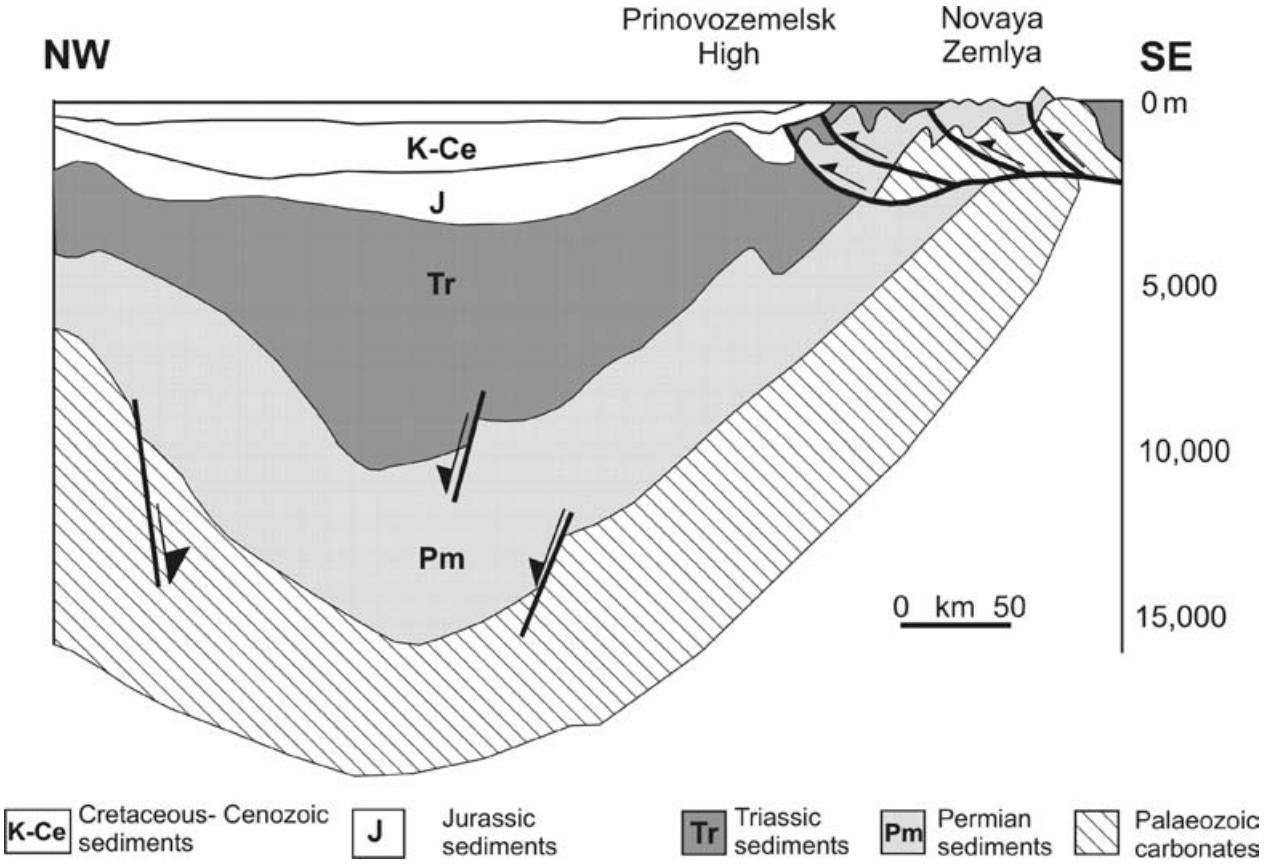

Figure 7. Cross-section of the northern end of the South Barents Sea basin which illustrates structural relationship between Novaya Zemlya and the basin. See Figure 1 for location.

geological evidence which suggests that lithospheric extension may have played an important role in the evolution of the region, our primary method of investigation is an inverse method which determines the variation of extensional strain rate as a function of time. The basin modelling techniques are outlined below but for a more thorough account the reader is referred to White (1994).

The first step in subsidence analysis is to calculate the water-loaded subsidence, thus isolating the tectonic component of subsidence. Each stratigraphic section is backstripped and water-loaded using standard techniques (Steckler & Watts, 1978). For sandstones and shales, we have used the initial porosities and decay lengths of Sclater & Christie (1980). For carbonates, we have used Schmoker & Halley's (1982) values. Realistic uncertainties in these compaction parameters have a minimal effect upon our results.

The lithosphere is assumed to respond to loading in an Airy isostatic manner. Admittance studies from other extensional sedimentary basins, such as the North Sea (Barton & Wood, 1984), and from passive continental margins (e.g. Fowler & McKenzie, 1989) suggest that continental lithosphere within an extensional setting has an elastic thickness, τ_e, of less than 5 km. If τ_e is small and if the load wavelength is ≤ 20 km, then Airy isostasy is a reasonable approximation.

Calculated water-loaded subsidence must be corrected for changes in palaeobathymetry (that is, the depth of water within which each sedimentary unit was deposited) and for changes in global sea-level variation. Palaeobathymetric estimates are crucial since each depositional unit does not generally fill a basin to sea-level. Estimates have been made using facies descriptions and biostratigraphic information (N. A. O'Leary, unpub. Ph.D. thesis, Univ. Cambridge, 1996). Fortunately, much of the stratigraphic succession consists of photic zone carbonates and evaporites (Fig. 3). Where present, clastic sedimentary rocks are generally shallow marine, deltaic or continental. Thus, for our purposes, much of the succession has relatively small uncertainties in palaeobathymetry (0–200 m or better). The depth of deposition for Permian foreland basin deposits is more difficult to constrain and so the associated uncertainty is larger (N. A. O'Leary, unpub. Ph.D. thesis, Univ. Cambridge, 1996).

Water-loaded subsidence data must also be corrected for global sea-level variation since subsidence calculations generally use present-day sea-level as a datum. Sea-level has undoubtedly varied throughout geological time but there is considerable debate about the magnitude and wavelength of this variation during the bulk of the Phanerozoic era. Wooler, Smith &

https://doi.org/10.1017/S0016756804008908 Published online by Cambridge University Press

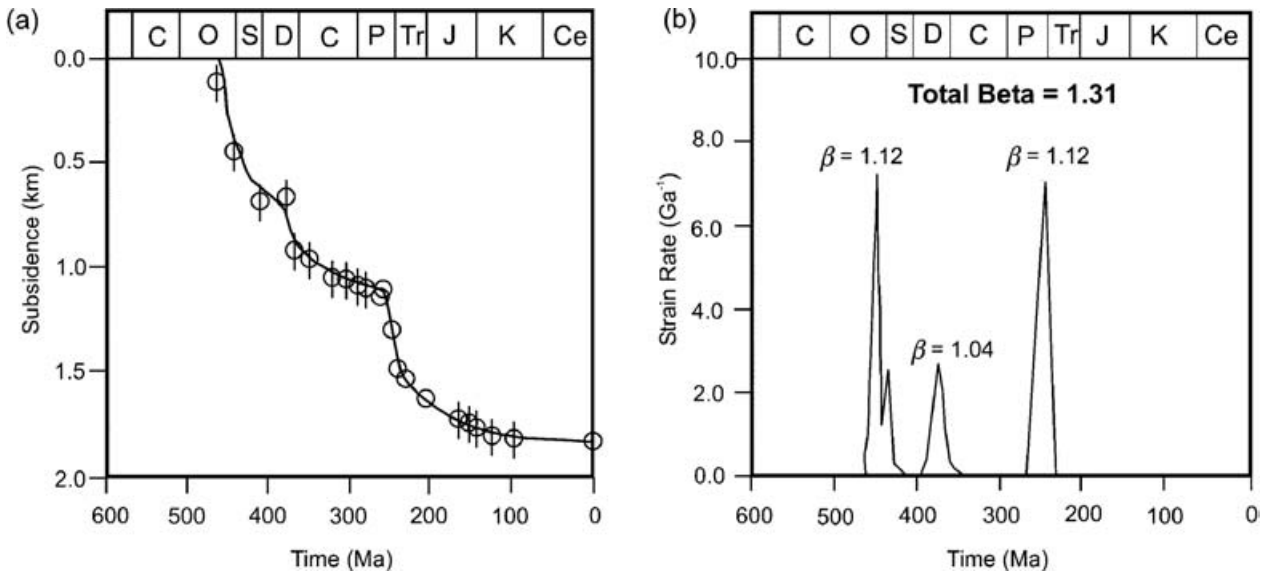

Figure 8. One-dimensional strain rate inversion of Section 71 (well Khoreyver-1). (a) Data points for water-loaded observed subsidence, calculated by standard backstripping method (Sclater & Christie, 1982); vertical bars represent uncertainty in water depth at time of deposition. Best-fitting theoretical subsidence curve is shown, calculated by allowing strain rate to vary smoothly as a function of time. There are three periods of extension separated by interludes of exponentially driven thermal subsidence. (b) Strain rate distribution as a function of time which yields theoretical subsidence curve shown in (a). Stretching factors for each of three rifting periods are given.

White (1992) showed the effect of adding various different published sea-level curves to water-loaded subsidence data from the Dolomites of Italy. They noted that the addition of most published eustatic curves resulted in poorer fits between observation and theory. Furthermore, inclusion of these sea-level curves generates periods of negative subsidence (uplift) at times when the stratigraphy clearly demonstrates that shallow-water subsidence occurred. Negative slopes on subsidence plots have no obvious physical meaning since they require 'negative rock'. This non-physicality implies that the amplitudes and wavelengths of existing Phanerozoic sea-level curves are incorrect. In this study, we encountered similar problems and so no sea-level corrections have been applied to the data shown in Figures 8 and 9.

Table 1. Parameters used in text; other parameters are given in White (1994)

Symbol	Parameter	Value (units)
a	Lithospheric thickness	120–125 km
t_c	Pre-rift thickness of continental crust	km
G	Lithospheric strain rate	s^{-1}
u	Horizontal advective velocity	km s^{-1}
v	Vertical advective velocity	km s^{-1}
β	Stretching factor	
τ_e	Lithospheric elastic thickness	km
D	Lithospheric flexural rigidity	Nm
S	Tectonic subsidence (water-loaded)	km
T	Temperature	°C
T_1	Temperature at base of lithosphere	1333 °C
α	Lithospheric thermal expansion coefficient	3.28×10^{-5} °C^{-1}
κ	Thermal diffusivity of the lithosphere	8.04×10^{-7} m^2 s^{-1}

3.b. Inverse modelling

In this section, we describe how decompacted and water-loaded subsidence data have been inverted using the strain rate inversion algorithm of White (1994) in order to determine the best-fitting strain-rate distribution (also see Table 1). This inversion scheme is based on the finite-duration lithospheric stretching model of Jarvis & McKenzie (1980). Using this finite-duration model, previous workers have calculated theoretical subsidence curves as a function of β, the stretching factor. Such forward modelling assumes that the strain rate, $G(t)$, is constant during rifting (that is, $\beta = \exp(G\Delta t)$ where Δt is the duration of stretching). The number and duration of rift events are determined from independent geological observations.

Sedimentary basins record vertical motion as a function of time, therefore the temporal variation in strain rate can be determined from a basin's subsidence history. An inverse model to extract the variation in strain rate with time from subsidence data was developed by White (1993). This method requires no *a priori* information about either the duration of rifting or the total strain. Error analysis shows that uncertainties in decompaction, palaeobathymetry and chronostratigraphy do not significantly alter the recovered strain rate histories (White, 1994). This method is robust in the presence of noise because considerable smoothing is applied. During extension, the vertical strain rate at the base of the lithosphere is

https://doi.org/10.1017/S0016756804008908 Published online by Cambridge University Press

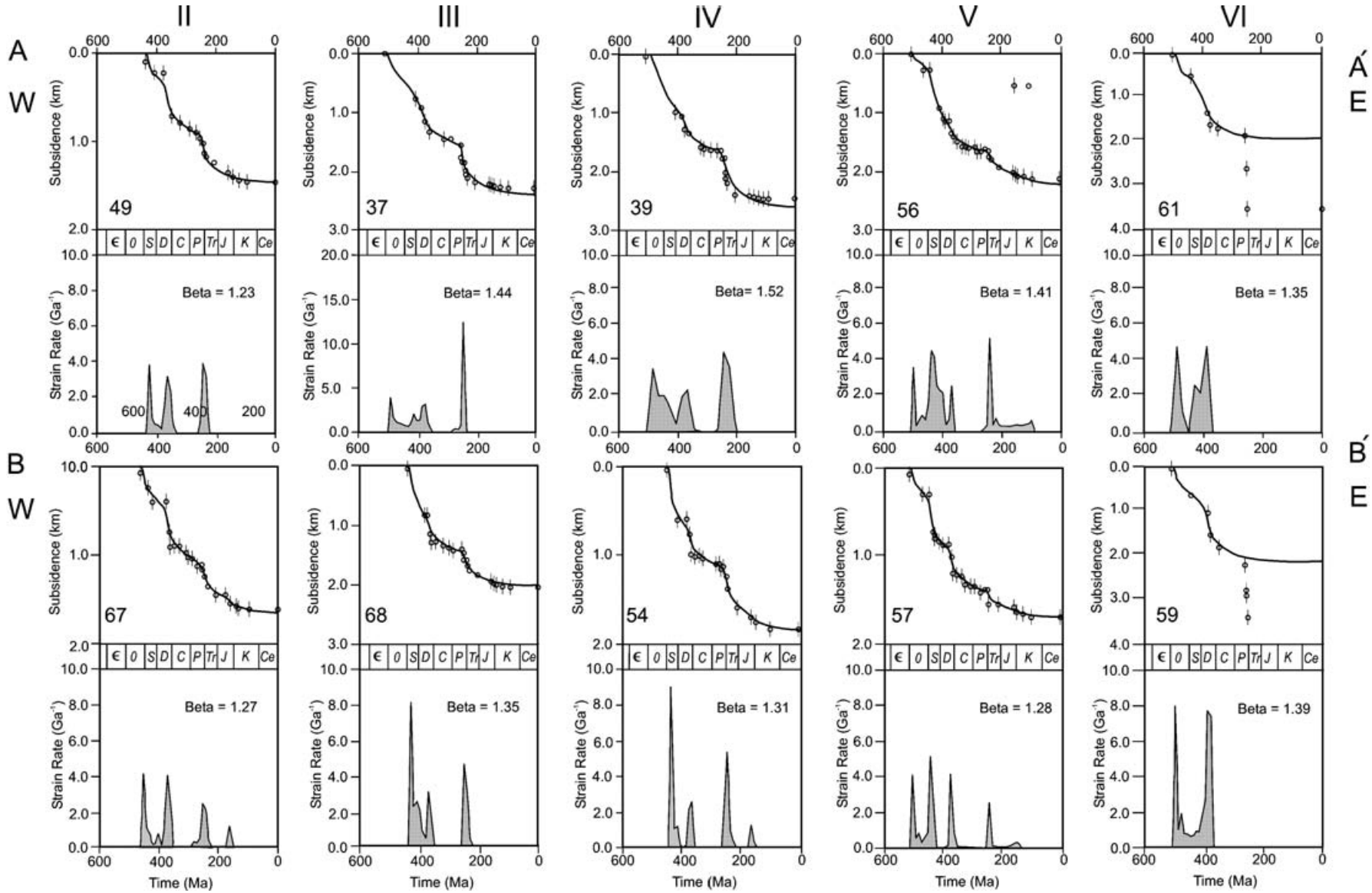

Figure 9. See legend on following page.

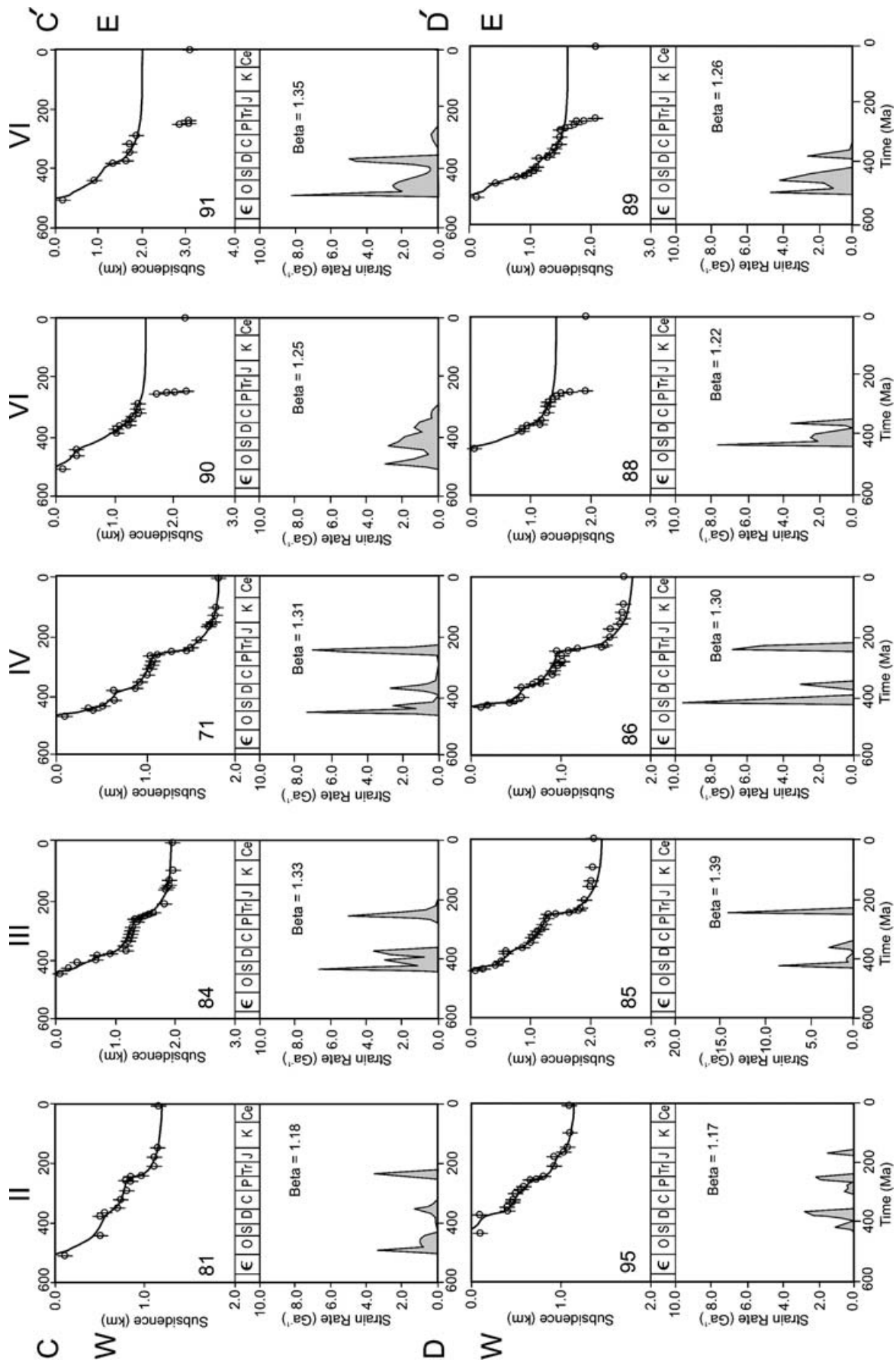

https://doi.org/10.1017/S0016756804008908 Published online by Cambridge University Press

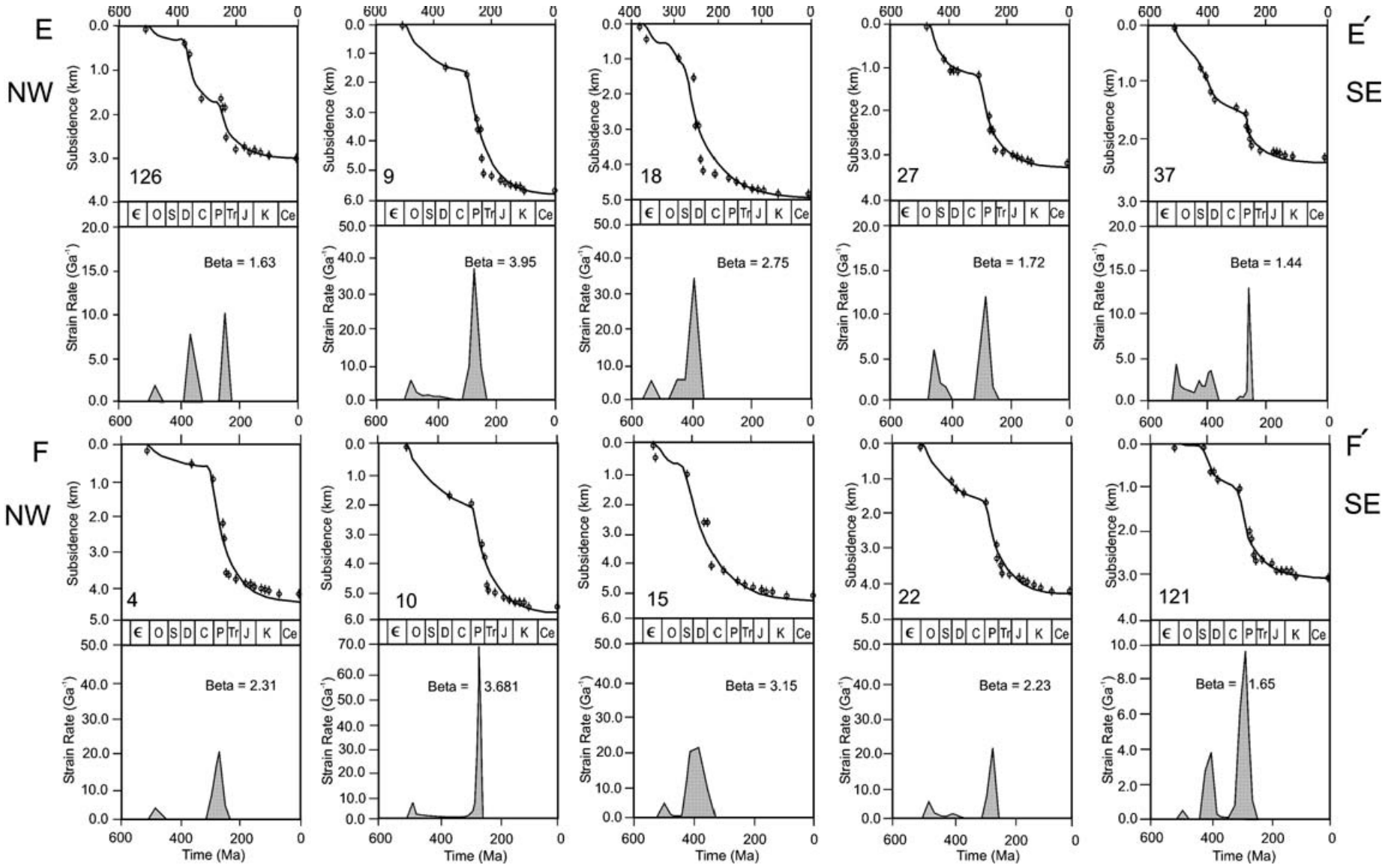

Figure 9. Six west-to-east transects of inverted stratigraphic sections from the Timan–Pechora and South Barents Sea basins (see Figs 1 and 2 for locations). Note that Permo-Triassic subsidence of foreland basin sections (structural zone V1) has not been modelled (see text for details). Subsidence and strain rate scales vary. Numbers in lower left of upper boxes are well locations.

assumed to be equal to the horizontal strain rate. For variable strain rate, the relationship between strain rate and β is given by

$$\beta = \exp\left(\int_0^t G(t)\,dt\right) \tag{1}$$

where $G(t)$ is the vertical strain rate. The relationship between $G(t)$ and subsidence, $S(t)$, is given by

$$S(t) = A(1 - 1/\beta) - B\,Q(t) \tag{2}$$

where

$$A = t_c(\rho_m - \rho_c)/(\rho_a - \rho_w), \tag{3}$$

$$B = \alpha\rho_m/(\rho_a - \rho_w), \tag{4}$$

and

$$Q(t) = \int_0^a [T(z,t) - T(z,\infty)]\,dz \tag{5}$$

$T(z,t)$ is the temperature of the lithosphere as a function of depth and time and $T(z,\infty)$ is the equilibrium temperature structure of the lithosphere. The symbols and values for other parameters are given in White (1993). $Q(t)$ is a measure of the difference between the perturbed and equilibrium temperature structure and is necessarily a function of $G(t)$. A and B are crustal thinning and lithospheric mantle thinning factors, respectively, and for the purposes of this paper are set to be constant (White, 1993).

The forward problem determines $S(t)$ from $G(t)$ and, as White (1993) has shown, is a straightforward calculation. Here we are interested in solving the more difficult inverse problem. For discrete and noisy data, the inverse problem is best solved by calculating a large number of forward models, varying only $G(t)$ each time until the difference between the theoretical subsidence curve and the data is minimized. $G(t)$ is first parameterized by using M discrete values, G_k, at time intervals δt, where δt is normally 5–10 Ma. $G(t)$ can then be obtained by interpolation between each time step. It is necessary to impose smoothing on $G(t)$ in order to stabilize inversion. Since the problem is non-linear and since all values of G should be greater than 0, a trial function, H, is minimized by systematically varying each value of G_k, using one of many search algorithms. H is given by

$$H = \left[\frac{1}{N}\sum_{i=1}^{N}\left(\frac{S_i^o - S_i^c}{\sigma_i}\right)^2\right]^{1/2} + W_1\left[\frac{1}{M-1}\sum_{k=2}^{M}\left(\frac{G_k - G_{k-1}}{\delta t}\right)^2\right]^{1/2} + W_2\left[\frac{1}{M}\sum_{k=1}^{M}\left(G_k''\right)^2\right]^{1/2} + \frac{W_3}{M}\sum_{k=1}^{M}|\log(G_k)| \tag{6}$$

where S_i^o and S_i^c are the observed and calculated subsidences used for inversion. N are the number of observations of subsidence and W_1, W_2, and W_3 are weighting coefficients. G_k'' are estimates of the second derivative of G generated by cubic spline interpolation. The first term on the right-hand side of the above equation is zero when calculated and observed values of S_i agree for all of the subsidence data. Dividing the difference between them by σ_i, the standard deviation, causes each term in the summation to have unit variance. The second and third terms cause $G(t)$ to be smooth and the fourth term tends to ∞ smoothly as any G_k approaches 0. All of the results discussed below were obtained with $W_1 = 0.5$, $W_2 = 0.5$, and $W_3 = 0.05$–0.5. H is an *ad hoc* function and it is very important to determine how results change with different values of the weighting coefficients. Varying the values of W_1 and W_2 by several orders of magnitude has a negligible effect but if they are set to zero, very rough solutions are sometimes obtained. W_3 must be greater than zero at the start of the inversion procedure but can subsequently be decreased to ensure that strain rates are allowed to approach zero in, for example, any post-rift periods.

The advantage of inverse modelling is that no assumptions regarding the timing, duration or magnitudes of rift events are required. However, once rift periods have been determined they must be confirmed by independent geological information about the growth of normal faults, crustal thinning and syn-rift magmatism. An important advantage of the inverse approach is that observational errors (e.g. in compaction, palaeobathymetry, chronostratigraphy) can be mapped into strain rate errors. Although we do not discuss error analysis here, previous work has demonstrated that strain rates can be determined to within at least one half of an order of magnitude (White, 1993).

The algorithm used here is one-dimensional and necessarily assumes that Airy isostasy applies (that is, the elastic thickness of the lithospheric plate, τ_e, is zero). There is considerable debate about the range of values of τ_e for continental lithosphere. Here, we have not attempted to determine τ_e for the Timan–Pechora and South Barents Sea basin. Instead, we justify an Airy isostatic assumption by referring to the results of Bellingham & White (2000).

They have taken a more rigorous approach than we have by developing a two-dimensional algorithm which includes potentially important two-dimensional effects such as lateral heat flow and flexural rigidity. Two-dimensional inversion of basin cross-sections using different values of τ_e suggests that many extensional sedimentary basins have elastic thicknesses of less than 5 km. They also showed that underestimating τ_e has a much smaller effect upon the calculated strain rate pattern than overestimating τ_e which can lead to serious discrepancies. We conclude that our results would not be very different if we had used small values of τ_e.

https://doi.org/10.1017/S0016756804008908 Published online by Cambridge University Press

4. Results of subsidence modelling

All 129 stratigraphic sections have been inverted to determine the temporal variation of strain rate. A sub-set of these data is presented. In the majority of cases, well-log information constrains the bulk of the stratigraphy. When a well has failed to penetrate to Precambrian basement, depth to basement and to other significant Palaeozoic horizons has been determined from seismic reflection profiles or from magnetic data.

A typical example of a modelled subsidence curve is shown in Figure 8. The Khoreyver-1 well (Section 71) is located in the centre of the basin and has recorded all of the important subsidence events. Palaeobathymetric uncertainties are relatively small (0–200 m at most). The theoretical subsidence curve fits the observed profile very well (Fig. 8a). This curve was generated by the strain rate pattern shown in Figure 8b. Peaks in strain rate indicate periods of rifting and the values of β were calculated directly from the strain rate distribution. The inverted data suggest that three main periods of rifting occurred, although it could be argued that the first period is a composite of two events. Ordovician and Permian–Triassic rifting events are small ($\beta \sim 1.1$) but more significant than Devonian rifting which is very mild ($\beta = 1.04$). The rift events are followed by thermal subsidence when strain rate decreases to zero. From mid-Triassic times until the present day, the observed subsidence is accurately modelled by simple thermal subsidence and there is no evidence for anomalous subsidence excursions caused by foreland or sub-lithospheric loading. In comparison with a global database of subsidence data, Section 71 is unusual in having recorded a large number of events (Newman & White, 1999).

4.a. Timan–Pechora basin

The density of subsidence profiles enables basin transects to be constructed. In Figure 9a–d, four transects of inverted subsidence curves are shown (see Fig. 1 for locations). Each stratigraphic section was selected based upon data quality and geographical location but can be regarded as typical of nearby sections. All four transects show a series of subsidence events which are consistent with multiple rifts. In general, there is evidence for three rifting periods although individual sections sometimes have more complex histories. The mean values of the start and finish of rift periods along with associated values of β are detailed in Table 2 and Figure 10. This summary was generated using the entire onshore Timan–Pechora database with the exception of sections located within the Uralian foreland basin. For the purpose of this study, a rift event is defined by strain rates greater than 0.1 Ga^{-1} (that is, 3.17×10^{-18} s^{-1}).

Table 2. Summary of rift events in Timan–Pechora basin

Rifting period (Ma)	Stratigraphic age	β
507–464	Tremadoc-Llandeilo	1.12
450–414	Caradoc-Ludlow	1.16
383–363	Middle-Late Devonian	1.06
264–242	Rotliegendes-Scythian	1.07

Mean values calculated using on-shore database and excluding sections located within Uralian foreland basin. Stratigraphic ages taken from Harland *et al.* (1989).

The first event is usually of Ordovician–Silurian age and, within the limitations of the data, is observed throughout the basin. Peak strain rate varies between 3 and 8 Ga^{-1} which yields βs of 1.1–1.2. We must emphasize that Ordovician–Silurian stratigraphy is the most poorly constrained, and sedimentary rocks of this age are only preserved with the rift zones themselves where total sediment thicknesses could reach ~ 7 km. In these zones, drilling does not usually penetrate basement. There is also a general lack of seismic reflection horizons as a result of the uniformity of the carbonate succession. This paucity of data has resulted in a large variation in rift duration. None the less, where wells have been drilled to basement, Ordovician rifting can be accurately constrained and appears to have lasted ~ 20 Ma (e.g. Sections 56 and 57). In some locations, there is evidence for a composite rift event (e.g. Section 89).

The second event occurred in Middle Devonian times and is usually the smallest: peak strain rates are ~ 2 Ga^{-1} and $\beta < 1.1$. This event is also seen throughout the basin but it is much better constrained since the Devonian section is penetrated by many wells.

The subsidence record for Permo-Triassic times onwards is the best constrained and also the most interesting. Within structural zones II, III and IV, there is clear evidence in favour of a final rift event centred on the Permo-Triassic boundary. This event is the most consistently identified across the whole dataset. It suggests that rifting was smallest at the western edge of the basin, increasing eastwards to reach a maximum within structural zone IV. This increase is most clearly illustrated by transect C. Peak strain rate on Section 81 is < 2 Ga^{-1}, increasing to ~ 6 Ga^{-1} on Section 84, and reaching ~ 8 Ga^{-1} on Section 71 (Fig. 9c). In each case, theory and observation are in good agreement, with little residual misfit. This agreement suggests that uniform lithospheric extension can account for the pattern of Permo-Triassic to present-day subsidence. Minor increases in Middle Jurassic subsidence (e.g. Sections 54 and 67) may represent a very mild, final rifting episode ($\beta \sim 1.02$).

The mean values of the timing of rifting, the corresponding stratigraphic intervals and the associated stretching factors are detailed in Table 2. These results

https://doi.org/10.1017/S0016756804008908 Published online by Cambridge University Press

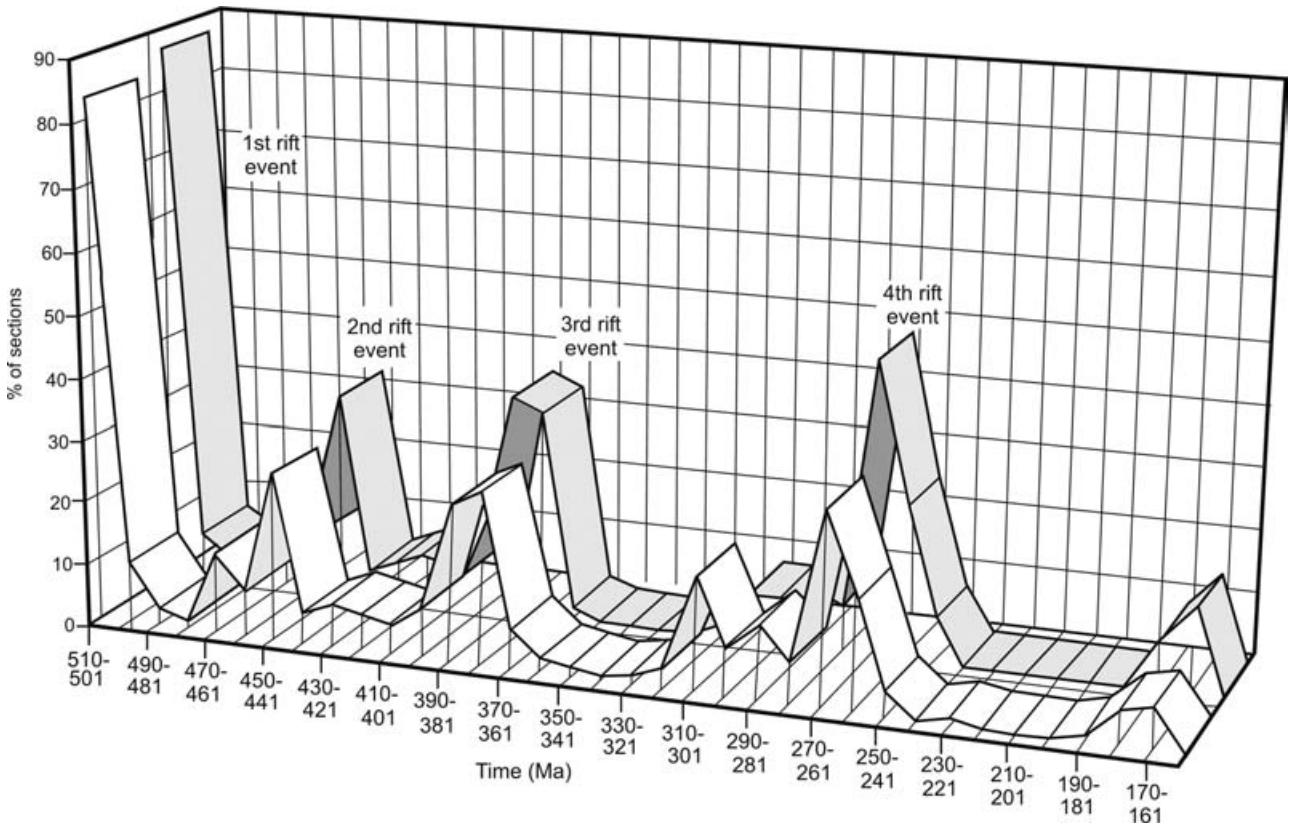

Figure 10. Percentage of stratigraphic sections which show rifting over last 500 Ma (bin size = 10 Ma). White curve in foreground = distribution for all stratigraphic sections; grey curve in background = distribution for sections derived from well-log information alone. Rift event is defined by strain rate values which exceed 0.1 Ga^{-1} (3.18×10^{-18} s^{-1}).

have been generated using the entire onshore Timan–Pechora database with the exception of sections located within the Uralian foreland basin.

The pattern of Permo-Triassic to Recent subsidence within structural zones V and VI cannot be so easily modelled. There are two important problems which are most clearly seen on Sections 59 and 61 (Fig. 9). Here, Permo-Triassic subsidence is extremely rapid and cannot be fitted by strain rate inversion unless peak strain rate and thus β are unacceptably large. Following Triassic times, there is a significant unconformity which is usually blanketed by Quaternary sediments. Thus thermal subsidence profiles observed tens of kilometres to the east are absent. On its own, this significant unconformity does not rule out Permo-Triassic rifting since later uplift and denudation could have occurred, removing the record of the thermal subsidence phase. However, the association of extremely rapid subsidence, which is $\sim$10 times faster than expected within a rift setting and often has a convex-upward shape on time-subsidence diagrams without thermal subsidence, suggests that this part of the Timan–Pechora basin formed by foreland loading. Our modelling implies that foreland loading is confined to a narrow strip along the western edge of the Ural Mountains.

4.b. South Barents Sea basin

Data from the South Barents Sea basin are less well constrained than for the Timan–Pechora basin. Depth to magnetic basement locally exceeds 20 km, although the average depth of our sections is $\sim$13 km (Johansen *et al.* 1992). These thicknesses compare to an average of 5 km from the onshore Timan–Pechora basin and adjoining continental shelf. Consequently, information about the Palaeozoic succession is mainly obtained from seismic reflection datasets. Extrapolation is especially difficult for the Lower Palaeozoic section where there are few seismic reflections and substantial gaps between data points. As a result, the data sampling interval for strain rate inversion has been increased to 20 Ma with a consequent loss in strain rate resolution. Some indication of the nature of the Palaeozoic sedimentary rocks of the South Barents basin can be obtained by extrapolating well data from Kolguyev Island, which show a similar succession to that seen for the onshore Timan–Pechora basin (Figs 1, 2).

The Upper Palaeozoic and Mesozoic section does not present such a problem: deep boreholes combined with key seismic horizons in the Devonian, Carboniferous, Permo-Triassic, Jurassic and Cretaceous

https://doi.org/10.1017/S0016756804008908 Published online by Cambridge University Press

permit satisfactory correlation. However, due to the substantial thicknesses of Permo-Triassic (up to 11 km) and Jurassic–Cretaceous (up to 3 km) strata, these boreholes usually give an insight into only the Mesozoic succession.

Figure 9e,f shows two subsidence transects across the South Barents Sea basin (see Fig. 1 for locations). The temporal data resolution is poorer than for the onshore Timan–Pechora basin and so it is difficult to constrain the Palaeozoic history. None the less, a few sections show increased subsidence rates, and hence strain rates, at similar times to the Timan–Pechora basin. Thus there is some evidence for Ordovician–Silurian rifting events (e.g. Sections 22 and 27). It is not possible to say whether this event represents one or two separate events, as is sometimes the case for the Timan–Pechora basin. The Middle–Late Devonian rift event is better constrained and is well represented in Sections 37, 121 and 126 (Fig. 9). What is most dramatically illustrated in the subsidence profiles is the extremely rapid subsidence from latest Carboniferous to earliest Triassic times (300–240 Ma). This subsidence event is penecontemporaneous with the Permo-Triassic event seen onshore, but yields much higher peak strain rates (up to 70 Ga^{-1}, equivalent to $2.2 \times 10^{-15}\,s^{-1}$) and thus higher stretching factors $\beta > 3$) than onshore. For these high values of β, the fits to data are not as good as those for the lower values of stretching seen onshore (compare Sections 18 and 37) but adequate fits have also been obtained (e.g. Sections 10 and 15). The significance of these events and possible association with onshore rifting will be discussed below.

5. Regional synthesis

It is important to integrate subsidence modelling within a general tectonostratigraphic framework. Results of our subsidence modelling suggest that the Timan–Pechora and South Barents Sea basins formed principally by multiple phases of rifting. There is also evidence which suggests that foreland loading accompanied rifting during Permo-Triassic times. Here, we consider how compatible these results are with independent geological and geophysical observations.

5.a. Palaeozoic rifting in Timan–Pechora

There is little doubt that the Palaeozoic succession in the Timan–Pechora basin is associated with rifting. Milanovsky (1981) reported Riphean rifting which is manifested by a NW–SE Baykalian basement trend of normal faults (Fig. 2). On the other hand, Johansen *et al.* (1992) have proposed a latest Precambrian–Early Cambrian origin for these faults. Both authors agree that these basement lineaments were later re-activated and have had a major influence on the tectonic evolution of the overlying sedimentary cover. Our subsidence modelling identified strain rate peaks, indicative of rifting, in Early Ordovician times, followed by a further event in the Late Ordovician–Silurian. Zonenshain *et al.* (1990) proposed rifting in Ordovician time as a precursor to the opening of the Sakmarian Ocean. Otto & Bailey (1995) and Johansen *et al.* (1992) have reported E–W extension in the Cambrian as a precursor to sea-floor spreading and opening of the Uralian Ocean in Ordovician–Silurian times. We suggest that the first two modelled events represent rifting episodes which accompanied opening of the Uralian Ocean and subsequent passive margin formation. Stretching factors associated with this event are low (β 1.05–1.35), implying that the present-day basin was situated on the periphery of the ocean basin.

There is limited evidence that the South Barents Sea basin also rifted at this time (e.g. Sections 22 and 27), although temporal resolution is very poor since it relies upon interpreted and depth-converted seismic data. Seismic sections which cross the Timan–Pechora–South Barents Sea margin (e.g. Verba, 1984; Gramberg, 1988) show evidence for tilted and fault-bounded blocks with Ordovician–Devonian syn-rift infill. This observation implies that both basins have had a similar Early Palaeozoic structural history. Some regional cross-sections show that these basins were separated by a palaeohigh until Permian times (Johansen *et al.* 1992; Ostisty & Cheredeev, 1993).

The third modelled strain rate peak occurs in Middle–Late Devonian times. This event is widespread throughout the Russian Platform and is recorded in the Volga-Urals, Pri-Caspian and Dnieper-Donets basins. Its timing and occurrence have been corroborated by previous workers. The physical manifestations of this episode in the Timan–Pechora basin are basaltic magmatism at the beginning of the Late Devonian (Churkin *et al.* 1981; Ziegler, 1988), and the development of Late Devonian half-grabens (Malyshev & Udin, 1991). Data from the South Barents Sea basin are better constrained for the Middle–Late Devonian and show a similar pattern of subsidence, although this episode cannot be identified in all sections. Its timing coincides with a rift phase identified by Baturin *et al.* (1991). Johansen *et al.* (1992) and Gramberg (1988) studied seismic reflection profiles from the South Barents Sea–Timan–Pechora region which show extensional graben and half-graben of Early–Middle Devonian age overlain by onlapping Upper Devonian post-rift sedimentary rocks. Stretching factors calculated from the best-fitting strain rate profiles are greater in the South Barents Sea ($\beta = 1.10$–1.27) than onshore ($\beta = 1.01$–1.11). The coeval nature of this event suggests that the South Barents Sea and Timan–Pechora basins were structurally interlinked at this time.

Thus the existence of this extensional event throughout the region is not disputed although its relationship to

https://doi.org/10.1017/S0016756804008908 Published online by Cambridge University Press

the tectonic development of the area is uncertain. Back-arc extension in the Sakmarian Basin has been proposed for Middle Devonian times, coincident with the timing of rifting in both basins (Ziegler, 1988; Zonenshain *et al.* 1990).

5.b. Permo-Triassic extension and compression

Perhaps the most interesting phase of subsidence is the Permo-Triassic event. This event is observed throughout both basins and is generally well constrained. Subsidence data are particularly accurately modelled in the Timan–Pechora basin and yield a mean stretching factor of $\beta = 1.07$ (Table 2). Offshore in the South Barents Sea basin, a coeval event is recognized but strain rates and β factors are much higher (compare Fig. 9a–d with 9e,f). Along the eastern edge of the Timan–Pechora basin, this rifting history is clearly complicated by what appears to be foreland basin subsidence. This foreland basin was associated with the Uralian Orogeny and impinged upon the eastern margin of the Timan–Pechora basin, overprinting the earlier NW–SE-striking rift structures (Fig. 2). The foreland basin itself consists of a number of elongate, *en echelon*, sub-basins which are separated by transverse ridges (e.g. the Chernyshev Ridge and Vorkutskoye High; Fig. 2). These sub-basins migrated westwards through Early Permian to Triassic times and now reach some 100–150 km west of the Main West Urals Thrust (Otto & Bailey, 1995).

The foreland basin sequence itself is more poorly sub-divided than elsewhere and so there are relatively few data points in some cases (e.g. section 61). Features typical of these sections are extremely rapid Permo-Triassic subsidence with a convex-up geometry and the absence of the thermal subsidence phase seen further west. In most places, Triassic rocks lie beneath the Quaternary cover (structural zone VI; Fig. 4). This pattern is suggestive of a flexural rather than an extensional event. All sections located within the foreland sub-basins show this Permo-Triassic subsidence pattern. The variation seen in the water-loaded subsidence is useful in identifying the transition from the Timan–Pechora rift basin into the Uralian foreland trough, and also helps constrain the timing of initiation of foreland basin formation in relation to Uralian orogenesis.

Although we have backstripped and water-loaded stratigraphic sections within the foreland basin, our results should be treated with caution. Lithospheric flexure is thought to play a significant role in foreland basin development which contradicts our assumption of Airy isostasy. Thrusting and large-scale clinoformal infilling of the foreland basin may give spurious overestimates of the stratigraphic thickness recorded by boreholes. We have circumvented the problem of generating and modelling water-loaded subsidence within the foreland basin by setting strain rate to zero (Fig. 9e,f). Our subsidence data merely emphasize the shape, amplitude and timing of flexural subsidence. Comparison of subsidence analyses for sections internal to the foreland basin (structural zone VI) and those located further west emphasizes the rapid change in subsidence character with distance from the Ural Mountains. External to the foreland basin in structural zones II–V, Permo-Triassic subsidence patterns are characteristic of those from any extensional sedimentary basin. Peak strain rates and stretching factors are small but clearly increase from west to east. Significantly, the Permo-Triassic event is followed by gradual subsidence to the present day which can be accurately fitted by negligible strain rates, thus representing the pattern expected of thermal post-rift subsidence. The only exceptions occur where minor increases in Jurassic subsidence are observed. Early Palaeozoic strain rate patterns beneath the foreland basin conform with those seen elsewhere in the basin (e.g. Sections 59 and 89). Thus, prior to foreland loading, this region is indistinguishable from the Timan–Pechora basin *sensu stricto*.

Our most surprising result is that to the west of structural zone VI, Permo-Triassic subsidence appears to be consistent with lithospheric stretching. Previously, this time period has been regarded as a time of structural inversion and foreland basin development associated with the Uralian Orogeny. Some workers (e.g. Johansen *et al.* 1992; Ostisty & Cheredeev, 1993; Otto & Bailey, 1995) have also argued that rapid Permo-Triassic subsidence in the South Barents Sea basin is caused by extensional tectonics. Extension is also well documented from east of the Uralian front at this time, both in the West Siberian Basin and in the Kara Sea (e.g. Aplonov, 1988; Girshgorn, 1988). In the Timan–Pechora basin, the Uralian foreland basin overprints earlier rift structures on the eastern margin of the basin (Fig. 2) and its effect can be recognized in inverted stratigraphic sections from within this zone (Fig. 9, structural zone VI).

5.c. Extrapolation into South Barents Sea basin

An important issue is how the Uralian foreland basin extends further north. Does it follow the changes in strike of the fold and thrust belt as expected? Previous reconstructions have depicted the region west of Novaya Zemlya (that is, the eastern margin of the South Barents Sea basin) as the offshore continuation of this foreland basin (Ziegler, 1988; Zonenshain, Kuzmin & Natapov, 1990). However, regional seismic profiles do not show the anticipated foreland basin geometries (Baturin, Vinogradov & Yunov, 1991; fig. 7 of Johansen *et al.* 1992; fig. 4 of Otto & Bailey, 1995). Instead, there is clearly Permo-Triassic normal faulting together with significant extension and attenuation of the continental crust, probably in Late Permian times (Otto & Bailey, 1995). Shortening structures and westward-directed

https://doi.org/10.1017/S0016756804008908 Published online by Cambridge University Press

thrusts of Late Permian–Early Triassic age are evident on several profiles, but die out east of major inversion anticlines such as the Admiralty High, located some 100 km west of Novaya Zemlya (Fig. 1). Offshore, Novaya Zemlya represents the continuation of the Uralian foreland basin, and isopach maps of Permo-Triassic thickness would be expected to show eastward thickening from the South Barents Sea into the foreland basin zone. However, such thickening is not observed and sediment thicknesses increase away from Novaya Zemlya into the South Barents Sea basin where accumulations of over 10 km of Permo-Triassic strata occur (Fig. 7).

Subsidence modelling from the South Barents Sea basin yields high strain rate peaks in Early Permian times (Fig. 9). The spatial distribution of stretching factors mimics the sediment isopach data (Fig. 11). These stretching factors are much greater than in the Timan–Pechora basin, reaching values of $\beta > 3$ in the centre of the Barents Sea. Calculated stretching factors for this Permo-Triassic event are shown in Figure 7b and have a similar pattern to the isopach data with high β factors centred in the South Barents Sea basin, decreasing towards Novaya Zemlya. If this rapid subsidence event is related to rifting in the South Barents Sea, the Permo-Triassic succession represents an extremely thick syn-rift sequence. This inference is consistent with Zonenshain, Kuzmin & Natapov's (1990) proposal that the crust beneath the South Barents Sea is attenuated and 'sub-oceanic' in character. They suggested that a Devonian rifting event ($\beta = 1.10$–1.27) was responsible for thinning but it is more likely that the Permo-Triassic rift event is the principal cause. The timing of this subsidence episode also coincides with a rift event identified on seismic data (e.g. Baturin *et al.* 1991; Johansen *et al.* 1992; Otto & Bailey, 1995).

Thus the Permo-Triassic history of the whole region is one of coeval collisional and extensional tectonics. Foreland basin formation on the eastern margin of the Timan–Pechora basin was accompanied by significant extension offshore in the South Barents Sea basin and also, to a lesser extent, in the Timan–Pechora basin.

The North Barents Sea basin underwent a similar tectonic history to that which we have outlined for the South Barents Sea basin. Prior to the Late Permian, only a single basin existed in the region (Ostisty & Cheredeev, 1993), implying that Early to Middle Palaeozoic rifting was responsible for the formation of both basins. The basins were separated following uplift of the Ludlov Saddle in Triassic times as a consequence of late stage Uralian shortening (Ostisty & Cheredeev, 1993). This uplift event was preceded by rapid subsidence associated with the Permian rift phase which affected the whole Barents Sea basin. Regional profiles show that both the North and South Barents Sea basins have very similar structures and sedimentary

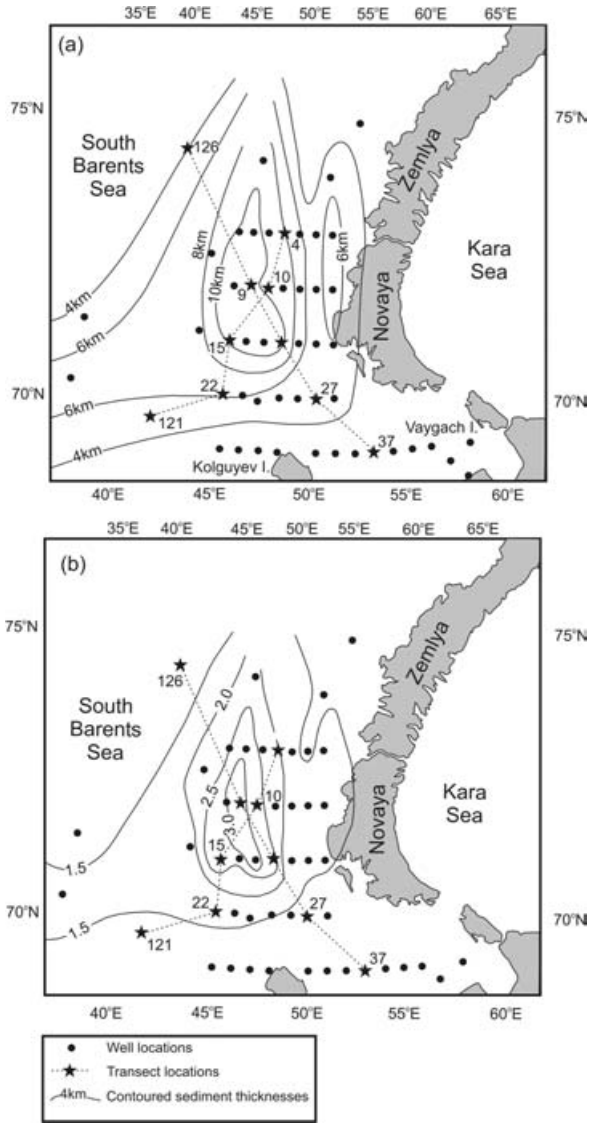

Figure 11. (a) Permo-Triassic isopach map of South Barents Sea basin, compiled from stratigraphic and seismic data (see also Johansen *et al.* 1992). Contours at 2 km intervals. Solid circles = location of stratigraphic sections (see also Fig. 1). Stars and dashed lines = transects E–E′ and F–F′ of Figure 9. (b) Map showing spatial distribution of stretching factor, β, for Permo-Triassic subsidence event.

thicknesses (Johansen *et al.* 1992; Figs 8, 11). Hence, not only is the mode of formation of the North Barents basin similar to that proposed for the South Barents basin but the stretching factors associated with the Permo-Triassic extension are also similar.

5.d. Mesozoic events

Otto & Bailey (1995) recognized northward thickening of the Mesozoic succession in the Timan–Pechora basin and suggested that it was the distal edge of thermal subsidence within the eastern South Barents Sea. Evidence for reactivation of normal faults in the

https://doi.org/10.1017/S0016756804008908 Published online by Cambridge University Press

Varandey–Adz'inskaya zone is association with basaltic volcanism (Kalantar *et al.* 1982; Fig. 2). The results of subsidence modelling suggest that active, though minor, extension and not just passive thermal subsidence, occurred in Permo-Triassic times. However, the rifting observed in the Timan–Pechora basin was probably causally related to the major rifting event identified in the South Barents Sea basin, with extension of the latter encouraging reactivation and renewed subsidence in the Timan–Pechora basin. In post-Triassic times, the entire region was tectonically quiescent, and post-rift thermal subsidence generated a thick Jurassic and Cretaceous succession which thins from the Barents Sea basin to the south into Timan–Pechora.

To resolve the problem of Permo-Triassic extension in the South Barents Sea basin and simultaneous shortening across Novaya Zemlya, Otto & Bailey (1995) suggested that this part of the Uralian fold and thrust belt was allochthonous. They suggested that Late Triassic thrusting of Novaya Zemlya was directed from the southeast over the margins of the South Barents Sea basin as a thin-skinned nappe (Fig. 7). The proposed allochthonous nature of Novaya Zemlya would explain why no significant foreland basin is imaged offshore to the west.

Baturin, Vinogradov & Yunov (1991) have suggested that a further rifting event occurred in the East Barents Sea during Late Jurassic–Early Cretaceous times. We note that minor increases in subsidence occur in the Middle Jurassic in the Timan–Pechora basin but β is only ~ 1.02. There is no evidence from the subsidence record to support the existence of this event in the South Barents Sea although a very minor event, such as seen onshore, could easily be masked by palaeobathymetric uncertainties. In addition, the strain rate inversion scheme is less sensitive in the late stages of analysis, resulting in poor modelling of the event anyway. Therefore, although rifting could have been occurring at this time elsewhere in the Barents Sea (as proposed by Johansen *et al.* (1992) for the westernmost basins offshore of Norway), there is no supporting evidence from subsidence data in the South Barents Sea basin. The very minor subsidence event seen in some sections in the Timan–Pechora basin during the Jurassic is anomalous, but mostly recognized offshore of Timan–Pechora, on the Pechora Block, and may represent minor reconfiguration, or tilting, of the Timan–Pechora–South Barents Sea margin.

6. Conclusions

In this study, we have used a large database of well-log and stratigraphic information to model the evolution of the Timan–Pechora and South Barents Sea basins. Our approach has focused on applying simple inverse basin modelling techniques to this database. The subsidence histories of both basins are most easily explained by intermittent phases of lithospheric extension. Theory and observation are generally in excellent agreement.

Calculated strain rate distributions identify at least four contemporaneous strain rate peaks corresponding to four periods of minor lithospheric extension in the Timan–Pechora basin in the Phanerozoic: Early Ordovician, Late Ordovician–Silurian, Middle–Late Devonian and Permian–Early Triassic times. Strain rate peaks from the South Barents Sea basin provide evidence for Ordovician–Silurian rifting, although the stratigraphic data supporting the existence of this event is poor and inadequately sampled and subdivided. Middle–Late Devonian extension in the South Barents Sea basin is better resolved and is supported by corroborating evidence from seismic reflection data. This event coincides with rifting in the Timan–Pechora basin and elsewhere in European Russia. Rapid rift-related subsidence also occurs in Permo-Triassic times with $\beta > 3$ in the centre of the basin. From a regional perspective, Early Palaeozoic extensional events are related to the opening of the Uralian Ocean and passive margin formation whilst Devonian rifting in both the Timan–Pechora and South Barents basins is coincident with the initiation of back-arc extension in the Sakmarian Ocean Basin (Zonenshain, Kuzmin & Natapov, 1990). We also suggest that the South and North Barents Sea basins share tectonic histories, at least for pre-Triassic times.

Our most important conclusion concerns the Permo-Triassic period. Along the western edge of the Timan–Pechora basin, subsidence data show that there is an anomalous departure from the behaviour associated with lithospheric extension. Water-loaded subsidence is at least one order of magnitude faster and often has a convex-upwards shape on our age-subsidence diagrams. Furthermore, the anticipated thermal subsidence is absent. We attribute this subsidence event to flexural loading associated with the Uralian Orogeny which resulted in eastward thrusting. This conclusion is neither new nor controversial. Further east, however, two sets of observations support the existence of coeval lithospheric extension. First, geological cross-sections demonstrate that stratigraphic growth occurred across normal faults during Permian–Early Triassic times. Secondly, Permian and younger subsidence is best accounted for by a phase of lithospheric stretching followed by post-rift cooling. This rifting episode occurs throughout most of the Timan–Pechora basin and can be followed north into the South Barents Sea basin. Seismic reflection, isopach and subsidence data all indicate that the Uralian foreland basin does not occur offshore of Novaya Zemlya. This observation supports the reconstructions of Otto & Bailey (1995), who favour an allochthonous origin for Novaya Zemlya.

It is difficult to account for simultaneous extension and shortening using conventional foreland basin

models. In their simplest form, these models explain foreland subsidence by the bending and loading of an elastic or visco-elastic beam (e.g. Turcotte & Schubert, 1982). Minor normal faulting away from the zone of foreland subsidence is consistent with the small amount of extension which will occur within the upper few kilometres of an elastic beam as it flexes. However, this extension is necessarily surficial. Our subsidence observations suggest that evidence for normal faulting is a consequence of minor stretching of the entire lithospheric plate. It is unclear how simultaneous lithospheric stretching and foreland loading can be explained by the standard elastic model. Instead, our results suggest that convective drawdown plays a role by pulling lithosphere toward the zone of maximum shortening.

Acknowledgements. NAO was supported by a NERC Ph.D. Studentship. Conoco, Exxon, JNOC, Mobil, Phillips and Texaco generously provided additional financial support. We are grateful to A. G. Smith and A. J. Butler for discussion, to J. Wardell for entering the data, and to S. Capon for drafting. A. Doré and R. Stephenson provided constructive reviews. Department of Earth Sciences Contribution Number 7471.

References

APLONOV, S. 1988. An aborted Triassic Ocean in West Siberia. *Tectonics* **7**, 1103–22.

BARTON, P. & WOOD, R. 1984. Tectonic evolution of the North Sea Basin; crustal stretching and subsidence. *Geophysical Journal of the Royal Astronomical Society* **79**, 987–1022.

BATURIN, D., VINOGRADOV, A. & YUNOV, A. 1991. Tectonics and hydrocarbon potential of the Barents Megatrough. *American Association of Petroleum Geologists Bulletin* **75**, 1404.

BELLINGHAM, P. & WHITE, N. 2000. A general inverse method for modelling extensional sedimentary basins. *Basin Research* **12**, 219–26.

BERGGREN, W. A., KENT, D. V., SWISHER, C. C. III & AUBRY, M.-P. 1995. A revised Cenozoic geochronology and chronostratigraphy. In *Geochronology, Time Scales and Global Stratigraphic Correlation* (eds W. A. Berggren, D. V. Kent, M.-P. Aubrey and J. Hardenbol), pp. 129–212. SEPM (Society for Sedimentary Geology) Special Publication no. 54.

CHURKIN, M., SOLEUMANI, G., CARTER, C. & ROBINSON, R. 1981. Geology of the Soviet Artic: Kola Peninsula to Lena River. In *The ocean basins and margins*, Volume 5 (eds A. E. M. Nairn, M. Churkin and F. G. Stehli), pp. 331–75. The Arctic Ocean. New York: Plenum Press.

DEDEYEV, V. A. 1982. *Struktura platformennogo chekhla evropeyskogo severa SSSR*. Leningrad, Nauka, 200 pp.

FOWLER, S. & MCKENZIE, D. 1989. Gravity studies of the Rockall and Exmouth Plateaux using SEASAT altimetry. *Basin Research* **2**, 27–34.

GIRSHGORN, L. SH. 1988. Riftogennye struktury severa Zapadnoy Sibiri. *Bulletin of Moscow State University Geological Division* **63**, 20–34.

GRAMBERG, I. 1988. *Barentsevskaya Sshel'fovaya Pilita*. Moscow: Nedra, 263 pp.

HARLAND, W. B., ARMSTRONG, R. L., COX, A. V., CRAIG, L. E., SMITH, A. G. & SMITH, D. G. 1989. *A geological timescale*. Cambridge: Cambridge University Press, 263 pp.

JARVIS, G. T. & MCKENZIE, D. P. 1980. Sedimentary basins formation with finite extension rates. *Earth and Planetary Science Letters* **48**, 42–52.

JOHANSEN, S. E., OSTISTY, B. K., BIRKELAND, O., FEDEROVSKY, Y. F., MARTIROSJAN, V. N., CHRISTENSEN, O. B., CHEREDEEV, S. I., IGNATENKO, E. A. & MARGULIS, L. S. 1993. Hydrocarbon potential in the Barents Sea region: play distribution and potential. In *Arctic geology and petroleum potential* (eds T. O. Vorren, O. A. Berager, E. Dahl-Stammes, B. Holter, E. Johansen, E. Lie and T. B. Lund), pp. 273–320. Norwegian Petroleum Society, Special Publication no. 2.

KALANTAR, I. Z., BUSHUYEV, A. S., UDOVICHENKO, L. A. & FIRER, G. M. 1982. Novyye dannye po stratigrafii i istorii geoligicheskogo Ezvitiya Varandey-Adz'vinskoy struktornoiy zony v pozdney permi i mezozoye. In *Syktyvkar: Komi Filial AN ASSR* (eds V. Molin and Y. E. Yudovich), pp. 87–91.

MALYSHEV, N. A. & UDIN, V. V. 1991. Structural style and evolution of the Pechora Basin, USSR. *American Association of Petroleum Geologists Bulletin* **75**, 1416.

MCKENZIE, D. P. 1978. Some remarks on the development of sedimentary basins. *Earth and Planetary Science Letters* **40**, 25–32.

MEYERHOFF, A. A. 1980. Petroleum basins of the Soviet Arctic. *Geological Magazine* **117**, 101–86.

MILANOVSKY, E. E. 1981. Aulacogens of ancient platforms: problems of their origin and tectonic development. *Tectonophysics* **73**, 213–48.

NEWMAN, R. & WHITE, N. 1999. The dynamics of extensional sedimentary basins: constraints from subsidence inversion. *Philosophical Transactions of the Royal Society, Series A* **357**, 805–34.

OSTISTY, B. K. & CHEREDEEV, S. I. 1993. Main factors controlling regional oil and gas potential in the west Arctic, former USSR. In *Basin modelling: advances and applications* (eds A. G. Dore *et al.*), pp. 591–7. Norwegian Petroleum Society, Special Publication no. 3

OTTO, S. C. & BAILEY, R. J. 1995. Tectonic evolution of the northern Ural Orogen. *Journal of the Geological Society, London* **152**, 903–6.

SCHMOKER, J. W. & HALLEY, R. B. 1982. Carbonate porosity versus depth. *American Association of Petroleum Geologists Memoir* **66**, 2561–70.

SCLATER, J. G. & CHRISTIE, P. A. F. 1980. Continental stretching: an explanation of the post-Mid-Cretaceous subsidence of the central North Sea Basin. *Journal of Geophysical Research* **85**, 3711–39.

STECKLER, M. S. & WATTS, A. B. 1978. Subsidence of Atlantic-type continental margin off New York. *Earth and Planetary Science Letters* **41**, 1–13.

TURCOTTE, D. & SCHUBERT, G. 1982. *Geodynamics: applications of continuum physics to geological problems*. New York: John Wiley & Sons.

VERBA, V. V. 1984. Comparative geological–geophysical characteristics of the Barents Sea and North Sea salt basins. *Petroleum Geology* **22**, 166–8.

WHITE, N. J. 1993. Recovery of strain rate variation from inversion of subsidence data. *Nature* **366**, 449–52.

WHITE, N. J. 1994. An inverse method for determining lithospheric strain rate variation on geological timescales. *Earth and Planetary Science Letters* **122**, 351–71.

WOOLER, D. A., SMITH, A. G. & WHITE, N. J. 1992. Measuring lithospheric stretching on Tethyan passive margins. *Journal of the Geological Society, London* **149**, 517–32.

ZIEGLER, P. A. 1988. Evolution of the Arctic-North Atlantic and the western Tethys. *American Association of Petroleum Geologists Memoir* **43**, 190 pp.

ZONENSHAIN, L. P., KUZMIN, M. I. & NATAPOV, L. M. 1990. *Geology of the USSR: a plate tectonic synthesis*. American Geophysical Union, Geodynamics Series 21. Washington, DC.

https://doi.org/10.1017/S0016756804008908 Published online by Cambridge University Press